Geometric Thermoelectric Pump: Energy Harvesting beyond Seebeck and Pyroelectric Effects

Jie Ren(任捷)*

Center for Phononics and Thermal Energy Science, China-EU Joint Lab on Nanophononics, Shanghai Key Laboratory of Special Artificial Microstructure Materials and Technology, School of Physics Science and Engineering, Tongji University, Shanghai 200092, China

(Received 25 June 2023; accepted manuscript online 8 August 2023)

Thermal-electric conversion is crucial for smart energy control and harvesting, such as thermal sensing and waste heat recovering. So far, researchers are aware of two main ways of direct thermal-electric conversion, Seebeck and pyroelectric effects, each with different working mechanisms, conditions and limitations. Here, we report the concept of Geometric Thermoelectric Pump (GTEP), as the third way of thermal-electric conversion beyond Seebeck and pyroelectric effects. In contrast to Seebeck effect that requires spatial temperature difference, GTEP converts the time-dependent ambient temperature fluctuation into electricity. Moreover, GTEP does not require polar materials but applies to general conducting systems, and thus is also distinct from pyroelectric effect. We demonstrate that GTEP results from the temperature-fluctuation-induced charge redistribution, which has a deep connection to the topological geometric phase in non-Hermitian dynamics, as a consequence of the fundamental nonequilibrium thermodynamic geometry. The findings advance our understanding of geometric phase induced multiple-physics-coupled pump effect and provide new means of thermal-electric energy harvesting.

DOI: 10.1088/0256-307X/40/9/090501

About 90 percent of the world's energy is utilized through heating and cooling, which makes energy waste a great bottleneck to the sustainability of any modern economy.[1] In addition to developing new technology of smart heat control,[2] the global energy crisis can be alleviated by recovering the wasted thermal energy. In view of the inconvenient truth that more than 60% of the energy utilization was lost mostly as wasted heat,[3] harvesting the thermal energy becomes critical to provide a cleaner and sustainable future.[1]

Thermal-electric energy harvesting mainly relies on two principles: Seebeck effect [Fig. 1(a)] and pyroelectric effect [Fig. 1(b)]. The Seebeck effect utilizes the spatial temperature difference between two sides of materials to drive the diffusion of charge carriers so as to convert heat into electricity.[4,5] Besides recovering waste heat, Seebeck effect with its reciprocal has wide applications of cooling, heating, power generating,[6] and thus has revitalized an upsurge of research interest recently.[7,8] However, when the ambient temperature is spatially uniform, we have to resort to the pyroelectric effect,[9] which utilizes the time-dependent temperature variation to convert heat into electricity but is restricted to pyroelectric materials.[10] This is due to the fact that the temporal temperature fluctuation modifies the spontaneous polarization of polar crystals, which consequently redistributes surface charges and produces temporary electric current.[11,12] In addition to thermal-electric energy harvesting,[13–17] pyroelectric effect has widespread applications in long-wavelength infrared sensing, motion detector, thermal image,[11] and even nanoscale printing.[18]

However, since Seebeck and pyroelectric effects have been known for quite a long time, one cannot help wondering: Does nature only offer us these two main means for thermal-electric energy harvesting? Does any new principle of thermal-electric conversion exist beyond them? The Seebeck effect has been known for 200 years,[19] and the pyroelectric effect, named in 1824,[20] can be even traced back to 314BC.[11] Now, it is time to think "out of the box", as advocated by Majumdar.[21]

In this work, we describe a third way of thermal-electric energy harvesting beyond Seebeck effect and pyroelectric effect, coined as Geometric Thermoelectric Pump (GTEP). This third way converts the time-dependent ambient temperature fluctuation into electricity [Figs. 1(c) and 1(d)], thus in contrast to Seebeck effect that requires spatial temperature difference. The third way is also distinct from pyroelectric effect in the sense that it does not require polar materials but applies to general conducting systems, although they produce the electricity in a similar manner [Fig. 1(d)]. This third way of thermal-electric conversion, i.e., GTEP, results from the charge redistribution through the temperature fluctuation and has a deep connection to the topological geometric phase in non-Hermitian dynamics.

The GTEP effect is similar to the geometric heat pump[22,23] and is a consequence of the fundamental nonequilibrium thermodynamic geometry. To illustrate the GTEP effect, we consider a typical nanodevice with only one electron level, as shown in Fig. 2(a). Although

*Corresponding author. Email: xonics@tongji.edu.cn
© 2023 Chinese Physical Society and IOP Publishing Ltd

we choose the single-level dot for demonstration due to the simplicity, it is worth emphasizing that the following discussions can be readily generalized to bulk materials. The mechanism of GTEP can be very general in periodically driven (and even stochastically driven) nonequilibrium systems with multiple-physics-coupled transports.

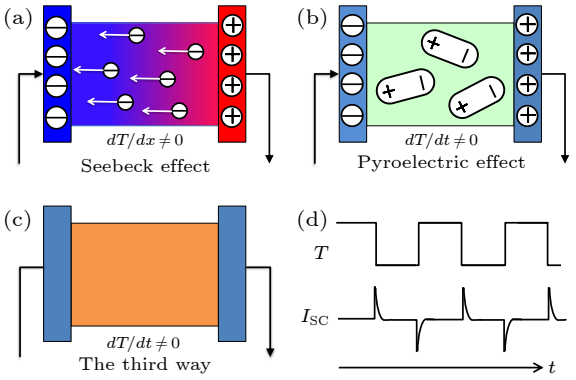

Fig. 1. Comparison of different thermal-electric conversion ways. (a) Seebeck effect converts the spatial temperature difference ($dT/dx \neq 0$) to electricity by driving the thermal diffusion of charge carriers from hot to cold. (b) Pyroelectric effect converts the temporal temperature variation ($dT/dt \neq 0$) to temporary electric current because variations of the temperature-dependent polarization in polar materials redistribute the surface charges. The typical behavior is similar to (d), also see Refs. [15–17]. (c) Distinctly, the third way, i.e., GTEP, produces electric current from the time-dependent temperature fluctuation in contrast to Seebeck effect, and it does not require polar materials but applies to general conducting system in contrast to pyroelectric effect. (d) The typical behavior of temperature-fluctuation-induced temporary electric current by the GTEP. It is in a similar manner as that of pyroelectric effect, also see Refs. [15–17].

The single-level nanodevice also has the great advantage of scalability and tunability, and it has many realizations such as single molecular junction, quantum dot, and quantum-point-contact systems that have shown promise for energy applications.[24–27] The transfer kinetics is described as follows:[28,29] An electron can hop from the $v(=L,R)$ lead into the single level with rate $\Gamma^v f^v$. When the level is occupied by an electron, the electron can escape to the v lead with rate $\Gamma^v(1-f^v)$. Here $f^v = [e^{(\varepsilon_0-\mu^v)/(k_{\rm B}T)}+1]^{-1}$ denotes the Fermi–Dirac distribution at the v lead with ε_0 being the energy of the single level. Γ^v is proportional to the system-lead coupling and the density of state of the lead v at ε_0, so that Γ^v is generally temperature-dependent.[30,31]

Periodic temperature fluctuation is imposed on the whole system, following Refs. [15–17]. Without loss of generality, we adopt the square-wave fluctuation that is convenient for theoretical analysis and can be decomposed as linear superpositions of periodic sine functions. The square-wave approximation is also justified since the temperature relaxation timescale in metallic leads can be very fast, even up to picosecond. Thus, once the fluctuation period is much larger than the relaxation time in metallic leads, the fluctuation can be safely approximated as an abrupt change. Moreover, we checked the fluctuation with smooth change, e.g., a single-frequent sine or cosine function. The results do not change qualitatively. In fact, any smooth (and even stochastic) temperature change protocols can be trotterized (decomposed) into step-wise discretized protocol.

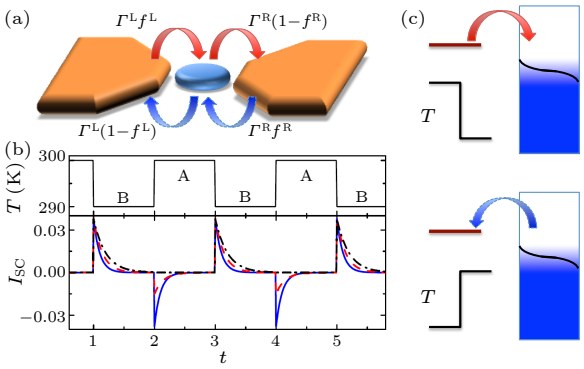

Fig. 2. The principle of GTEP effect of thermal-electric conversion from the ambient temperature fluctuation. (a) Sketch of the single-level nanodevice and its charge transfer dynamics. (b) Temperature-fluctuation-induced temporary electric current. Temperature varies between $T_{\rm A} = 300\,{\rm K}$ and $T_{\rm B} = 290\,{\rm K}$. Other parameters are $\varepsilon_0 = 40\,{\rm meV}$, $\Gamma^{\rm L}_{\rm A} = \Gamma^{\rm R}_{\rm B} = 5$, $\Gamma^{\rm R}_{\rm A} = \Gamma^{\rm L}_{\rm B} = 5$ (solid), 2 (dashed), 0 (dot-dashed). The latter two cases show that the asymmetric system-lead coupling variation rectifies the ac current. (c) Schematic illustration of the electron transfer through the right lead under temperature variation: When temperature decreases, the electron transfers from the central level to the lead. When temperature increases, the electron is injected from the lead to the central level. Results can be reversed if the system changes from hole-type ($\varepsilon_0 > 0$) to electron-type ($\varepsilon_0 < 0$). Similar phenomena can be found in bulk materials when transport changes from conduction band to valance band. GTEP effect will vanish in systems with electron-hole symmetry.

As such, the ambient temperature switches between high temperature $T_{\rm A}$ and low temperature $T_{\rm B}$, each with duration time $\mathcal{T}_{\rm p}$, as depicted in Fig. 2(b). Accordingly, the system's evolution can be divided into two ensembles, of which the two sets of parameters are denoted by the corresponding superscripts A and B, respectively. Without doubt, in either of two ensembles the system is in equilibrium with a homogenous temperature, which as is well understood can not produce electric current. However, as we will see, the electric current indeed emerges with the help of temperature fluctuations, because switching between two different equilibrium ensembles ultimately makes the whole evolution out of equilibrium. We set $\mu^v = 0$ so that $f^{\rm L}_{\rm A,B} = f^{\rm R}_{\rm A,B} = f_{\rm A,B}$ and focus on the short-circuit current through the right lead. Straightforward calculations lead us to the analytic expressions of temporary (short-circuit) electric currents:

$$I_{\rm SC} = \begin{cases} -\Gamma^{\rm R}_{\rm A}(f_{\rm A}-f_{\rm B})\frac{1-e^{-K_{\rm B}\mathcal{T}_{\rm p}}}{1-e^{-(K_{\rm A}+K_{\rm B})\mathcal{T}_{\rm p}}}e^{-K_{\rm A}\tau_{\rm A}}, \\ \Gamma^{\rm R}_{\rm B}(f_{\rm A}-f_{\rm B})\frac{1-e^{-K_{\rm A}\mathcal{T}_{\rm p}}}{1-e^{-(K_{\rm A}+K_{\rm B})\mathcal{T}_{\rm p}}}e^{-K_{\rm B}\tau_{\rm B}}, \end{cases} \tag{1}$$

where $K_u = \Gamma_u^{\rm L} + \Gamma_u^{\rm R}$ and $\tau_u =$ mod $(t \in u, \mathcal{T}_{\rm p})$ with $u = {\rm A}, {\rm B}$. The first (second) line of $I_{\rm SC}$ is the evolution expression of temporary electric current when $t \in \tau_{\rm A(B)}$ within the periods $\tau_{\rm A(B)}$ of A (B). Results of the GTEP effect are displayed in Fig. 2(b), which shows consistency with the thermal-electric generation of pyroelectric effect in a similar manner.[15–17]

The kinetics of the GTEP induced thermal-electric conversion can be understood as follows [also see Fig. 2(c)]: Before changing the temperature, the central system and the lead have built an equilibrium, thus no net charge transfers. However, when ambient temperature fluctuates to lower one, less electrons will populate above the lead's Fermi level since the thermal broadening will shrink. As such, the balance is broken and the electron tends to transfer from the central system to the lead and then relax to a new equilibrium. When temperature fluctuates back to higher one, more electrons will populate above the lead's Fermi level due to the thermal broadening. Thus, the redundant conduction electron in the lead will transfer to the central system, trying to build a new balance. Therefore, even without polar materials, the GTEP effect is able to generate electric current from the ambient temperature fluctuation in general conducting system, which is intrinsic to the nonequilibrium kinetics. Though with different principles, considering the similar generated electric current behaviors between the GTEP and pyroelectric effect,[15–17] we may use a full-wave bridge circuit to rectify the ac current,[16] which can also be achieved by the asymmetric system-lead coupling variation [Fig. 2(b)].

So far, we have shown that GTEP effect, the third way of thermal-electric conversion, is a consequence of the charge redistribution through the temporal temperature fluctuation. In the following, we will unravel its deep connection to the topological geometric phase in non-Hermitian quantum mechanics, as a consequence of the nonequilibrium thermodynamic geometry. The evolution of the system can be described by a Schrödinger equation in imaginary time, that is, a twisted master equation with the counting field χ:[22]

$$\frac{d}{dt}|\Psi_\chi(t)\rangle = \hat{H}(\chi, t)|\Psi_\chi(t)\rangle, \tag{2}$$

where $|\Psi_\chi(t)\rangle = \sum_{q=-\infty}^{\infty} e^{iq\chi}[p_0(q,t), p_1(q,t)]^{\rm T}$ with $p_{0/1}(q,t)$ denoting two joint probabilities that at time t the single level is empty or occupied by an electron while there have already q electrons transferred into the right lead. The transfer operation $\hat{H}$ is reminiscent of the Hamiltonian but non-Hermitian. In either $u = {\rm A}$ or B equilibrium ensemble, $\hat{H}$ is expressed as

$$\hat{H}_u = \begin{pmatrix} -K_u f_u & (\Gamma_u^{\rm L} + \Gamma_u^{\rm R} e^{i\chi})(1-f_u) \\ (\Gamma_u^{\rm L} + \Gamma_u^{\rm R} e^{-i\chi}) f_u & -K_u(1-f_u) \end{pmatrix}.$$

Therefore, after n fluctuation periods the evolution at time $t = 2n\mathcal{T}_{\rm p}$ is described by the characteristic function:

$$Z_\chi = \langle \mathbf{1}| \left[e^{\hat{H}_{\rm B}\mathcal{T}_{\rm p}} e^{\hat{H}_{\rm A}\mathcal{T}_{\rm p}} \right]^n |\Psi_\chi(0)\rangle \sim e^{n\Phi(\chi)} \tag{3}$$

with $\langle \mathbf{1}| = (1,1)$, which in turn generates the total electron transfer per period via the relation: $Q := \partial\Phi(\chi)/\partial(i\chi)|_{\chi=0}$ with the cumulant generating function defined as $\Phi(\chi) := \lim_{n\to\infty} \frac{1}{n} \ln Z_\chi$.

At the slow switch limit (large $\mathcal{T}_{\rm p}$), the evolution at either ensemble $\hat{H}_u$ ($u = {\rm A}$ or B) is dominated by the corresponding eigenmode, of which the eigenvalue λ_u has the largest real part, with $|\psi_u\rangle$ and $\langle\varphi_u|$ being the corresponding normalized right and left eigenvectors, such that $e^{\hat{H}_u\mathcal{T}_{\rm p}} \approx |\psi_u\rangle e^{\lambda_u\mathcal{T}_{\rm p}}\langle\varphi_u|$. Therefore, the characteristic function can be expanded as

$$Z_\chi(t) \approx e^{(\lambda_{\rm A}+\lambda_{\rm B})n\mathcal{T}_{\rm p}}[\langle\varphi_{\rm A}|\psi_{\rm B}\rangle\langle\varphi_{\rm B}|\psi_{\rm A}\rangle]^n C, \tag{4}$$

with $C = \langle\mathbf{1}|\psi_{\rm B}\rangle\langle\varphi_{\rm A}|\Psi_\chi(0)\rangle / \langle\varphi_{\rm A}|\psi_{\rm B}\rangle$ being an unimportant coefficient. This expansion of Z_χ gives the cumulant generating function $\Phi(\chi)$, composed of two contributions: $Z_\chi \sim e^{n\Phi(\chi)} = e^{n(\Phi_{\rm dyn}+\Phi_{\rm top})}$, with

$$\Phi_{\rm dyn} = (\lambda_{\rm A} + \lambda_{\rm B})\mathcal{T}_{\rm p}, \tag{5a}$$

$$\Phi_{\rm top} = \ln[\langle\varphi_{\rm A}|\psi_{\rm B}\rangle\langle\varphi_{\rm B}|\psi_{\rm A}\rangle]. \tag{5b}$$

Being reminiscent of the dynamic phase in quantum mechanics, we call $\Phi_{\rm dyn}(\chi)$ the dynamic phase contribution of the cumulant generating function, which presents the average evolution as if the system evolves in either ensemble separately, and then take a simple summation. As a consequence of the detailed balance at each equilibrium ensemble, the dynamic phase contribution to the electric-thermal conversion is always zero: $\partial\Phi_{\rm dyn}/\partial(i\chi)|_{\chi=0} = 0$.

The second part $\Phi_{\rm top}(\chi)$ however possesses a nontrivial topological geometric phase interpretation, which is responsible for the temperature-fluctuation-induced electron transfer. Different from the Hermitian Hamiltonian in quantum mechanics, the twisted transfer operator $\hat{H}_u$ are non-Hermitian such that its left eigenvector $\langle\varphi_u|$ is not the Hermitian conjugate of the corresponding right eigenvector $|\psi_u\rangle$, but only bi-orthonormal with each other. Therefore, writing $\langle\varphi_{\rm A}|\psi_{\rm B}\rangle = |\langle\varphi_{\rm A}|\psi_{\rm B}\rangle|e^{i\phi_{\rm AB}(\chi)}$ and $\langle\varphi_{\rm B}|\psi_{\rm A}\rangle = |\langle\varphi_{\rm B}|\psi_{\rm A}\rangle|e^{i\phi_{\rm BA}(\chi)}$ with angle $\phi_{\rm AB}$ and $\phi_{\rm BA}$ as the analogy of Pancharatnam's topological phase between discrete states,[32,33] we have $\phi_{\rm AB} \neq -\phi_{\rm BA}$ generally. As such, the transferred electron number per period resulting from this topological phase contribution is obtained as follows:

$$Q = \frac{\partial\Phi_{\rm top}}{\partial(i\chi)}\Big|_{\chi=0} = \frac{(f_{\rm A}-f_{\rm B})(\Gamma_{\rm A}^{\rm L}\Gamma_{\rm B}^{\rm R} - \Gamma_{\rm B}^{\rm L}\Gamma_{\rm A}^{\rm R})}{K_{\rm A}K_{\rm B}}. \tag{6}$$

This quantity only depends on the topological phase properties of $\langle\varphi_u|$ and $|\psi_u\rangle$, the left and right ground states of the non-Hermitian dynamics $\hat{H}_u$, and is independent of the period in the large $\mathcal{T}_{\rm p}$ limit, which looks similar to the behavior governed by the adiabatic Berry phase effect[34–41] with smooth and continuous driving protocols.

However, we note that here the Pancharatnam-like topological phase contribution is distinct from previous Berry phase studies,[36–39,42–44] where the temperature modulations had a phase lag so as to form a closed loop with non-zero area in the parameter space for the latter case. The Pancharatnam-like phase here actually denotes an isothermal non-adiabatic process due to the abruptly

discrete switching. The nonzero net charge transfer per period is kinetically offered by the nonequilibrium asymmetric relaxations between two equilibrium ensembles A↔B with different temperatures, which is characterized by the non-cancellation of phases of inner products $\langle\varphi_{\rm B}|\psi_{\rm A}\rangle$ and $\langle\varphi_{\rm A}|\psi_{\rm B}\rangle$ in the topological phase contribution $\Phi_{\rm top}$. This is distinct from those in quantum mechanics, where if having only two-state switching, $\phi_{\rm AB}$ will be always equal to $-\phi_{\rm BA}$,[33] leading to zero contribution. In Hermitian quantum mechanics, to avoid the cancelation of phases, at least three-state change was necessary to form a closed loop in the parameter space with nonzero area in order to get the nonzero contribution. Even in the continuous driven master equation with counting field, a nonzero area enclosed by the driving protocol in the parameter space was necessary to obtain a finite Berry's geometric phase contribution. Nevertheless, two-state switch here is already enough to generate finite charge transfer from the Pancharatnam-like phase through Eqs. (5b) and (6), even though the closed area of the driven protocol is zero in the parameter space, because $\langle\varphi_u|$ for non-Hermitian dynamics is not Hermitian conjugate of the corresponding right eigenvector $|\psi_u\rangle$. The similar phenomenon has also been demonstrated in temporally driven macroscopic thermal diffusion[23] in both theory and experiment. In Ref. [23], the connection between Trotterized discrete switching protocol (Pancharatnam's phase induced geometric heat pump) and continuous driving protocol (Berry's phase induced geometric heat pump) is discussed in detail.

At the fast switch limit (small $\mathcal{T}_{\rm p}$), we can approximate $\exp[\hat{H}_{\rm B}\mathcal{T}_{\rm p}]\exp[\hat{H}_{\rm A}\mathcal{T}_{\rm p}] \approx \exp[(\hat{H}_{\rm A}+\hat{H}_{\rm B})\mathcal{T}_{\rm p}]$. Denote $\lambda_{\rm AB}(\chi)$ as the dominated eigenvalue of the matrix $(\hat{H}_{\rm A}+\hat{H}_{\rm B})$, the solution at fast switch limit is obtained as

$$Q=\mathcal{T}_{\rm p}\frac{\partial\lambda_{\rm AB}}{\partial(i\chi)}=\frac{\mathcal{T}_{\rm p}(f_{\rm A}-f_{\rm B})(\Gamma_{\rm A}^{\rm L}\Gamma_{\rm B}^{\rm R}-\Gamma_{\rm B}^{\rm L}\Gamma_{\rm A}^{\rm R})}{K_{\rm A}+K_{\rm B}}. \quad (7)$$

Clearly, in this fast switch regime, Q is proportional to the half-period $\mathcal{T}_{\rm p}$, while the average current $Q/(2\mathcal{T}_{\rm p})$ becomes a period-independent constant.

In fact, by considering the characteristic function and the cumulant generating function in Eq. (3), the full exact solution of the total thermally generated electron transfer per period at arbitrary switch rate (i.e., arbitrary $\mathcal{T}_{\rm p}$) can be obtained as

$$\begin{aligned}Q=&\frac{\partial\Phi(\chi)}{\partial(i\chi)}|_{\chi=0}=\lim_{n\to\infty}\frac{1}{n}\frac{\partial\ln Z_\chi}{\partial(i\chi)}|_{\chi=0}\\=&\frac{(f_{\rm A}-f_{\rm B})(\Gamma_{\rm A}^{\rm L}\Gamma_{\rm B}^{\rm R}-\Gamma_{\rm B}^{\rm L}\Gamma_{\rm A}^{\rm R})}{K_{\rm A}K_{\rm B}}\\&\cdot\frac{(1-e^{-K_{\rm A}\mathcal{T}_{\rm p}})(1-e^{-K_{\rm B}\mathcal{T}_{\rm p}})}{(1-e^{-(K_{\rm A}+K_{\rm B})\mathcal{T}_{\rm p}})},\end{aligned} \quad (8)$$

which is also seen as the result from integrating Eq. (1) within one period: $Q=\int_0^{2\mathcal{T}_{\rm p}}dtI_{\rm SC}(t)$. Clearly, the relaxation factor $\frac{(1-e^{-K_{\rm A}\mathcal{T}_{\rm p}})(1-e^{-K_{\rm B}\mathcal{T}_{\rm p}})}{(1-e^{-(K_{\rm A}+K_{\rm B})\mathcal{T}_{\rm p}})}$ plays the key role in the transition behavior from slow-switch limit (≈ 1 when $\mathcal{T}_{\rm p}\gg 1/K_{\rm A},1/K_{\rm B}$) to fast-switch limit [$\approx\frac{K_{\rm A}K_{\rm B}}{K_{\rm A}+K_{\rm B}}\mathcal{T}_{\rm p}$, when $\mathcal{T}_{\rm p}\ll 1/(K_{\rm A}+K_{\rm B})$]. Therefore, the full exact solution in the small $\mathcal{T}_{\rm p}$ limit coincides with the fast switch result and in the large $\mathcal{T}_{\rm p}$ limit it reduces to the Pancharatnam-like topological-phase contribution Eq. (6). Therefore, the full exact solution in the large $\mathcal{T}_{\rm p}$ limit reduces to the Pancharatnam-like topological-phase contribution Eq. (6) and in the large $\mathcal{T}_{\rm p}$ limit it coincides with the fast switch result Eq. (7).

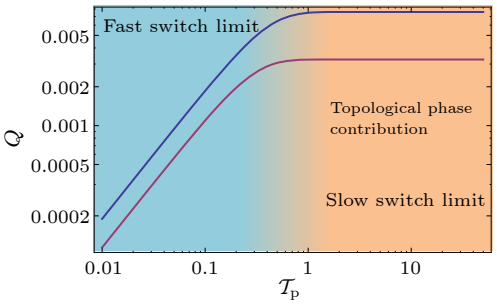

Fig. 3. The electron transfer generated per period by the GTEP effect of thermal-electric energy harvesting. The thermal-electric conversion in the slow switch limit has an interpretation of topological phase, and gives the upper bound of the thermal-electric conversion per period. $\Gamma_{\rm A}^{\rm R}=\Gamma_{\rm B}^{\rm L}=0$ (upper curve), 2 (lower curve). Other parameters are the same as those used in Fig. 2. For the maximal asymmetric coupling variation, the topological geometric phase contribution will reach a plateau $Q=f_{\rm A}-f_{\rm B}$ at large $\mathcal{T}_{\rm p}$, so that at large temperature fluctuation $f_{\rm A}\approx 1/2, f_{\rm B}\approx 0$, the geometric thermo-electric pumped charge will be half-quantized as $Q=1/2$.

As shown in Fig. 3, the topological-phase contribution in the slow switching gives the upper limit of the thermal-electric conversion per period by the GTEP effect. Intuitively, Q is proportional to $f_{\rm A}-f_{\rm B}$ that is in turn proportional to $T_{\rm A}-T_{\rm B}$, i.e., large temperature fluctuations produce more electricity. Moreover, Eq. (8) shows that Q is proportional to $\Gamma_{\rm A}^{\rm L}\Gamma_{\rm B}^{\rm R}-\Gamma_{\rm B}^{\rm L}\Gamma_{\rm A}^{\rm R}$. This indicates that the larger the asymmetric coupling variation $\Gamma_{\rm A}^{\rm L}/\Gamma_{\rm A}^{\rm R}\neq\Gamma_{\rm B}^{\rm L}/\Gamma_{\rm B}^{\rm R}$, the larger the electric generation. The largest asymmetry could be achieved by letting $\Gamma_{\rm A}^{\rm R}=0$ in the first half period, and $\Gamma_{\rm B}^{\rm L}=0$ in the second half period, see Fig. 3, which corresponds to the anti-phase transfer: in ensemble A the electron transfers from the left lead to the central system that decouples with the right lead (with probability $f_{\rm A}$); in ensemble B, the central system decouples with the left lead and the electron transfers from the central part to the right lead (with probability $f_{\rm B}$). As such, the geometric thermo-electric pumped charge is $Q=f_{\rm A}-f_{\rm B}$ at slow switch limit, which will be half-quantized as $Q=1/2$ when temperature fluctuation is large ($f_{\rm A}\approx 1/2$ at high temperature and $f_{\rm B}=0$ at low temperature). This picture also coincides with the largest rectification shown in Fig. 2(b) and is sketched in Fig. 2(c). Qualitatively similar effect has also been demonstrated in temporally driven macroscopic thermal diffusion both theoretically and experimentally.[23]

The same analysis can be applied to the nonequilibrium entropy production. Following Refs. [45–47], we can split the total entropy production into the system entropy production and the flux entropy production (i.e.,

the environment entropy production due to the dissipation of the transition flux), as $\dot{S}_{\rm tot} = \dot{S} + \dot{S}_{\rm flux} \geq 0$, where the second equality holds only in equilibrium in the absence of net transferred electric flux. After one full switching period $2\mathcal{T}_{\rm p}$ we see that the entropy change $\Delta S = \int_0^{2\mathcal{T}_{\rm p}} dt\dot{S} = 0$ because the system's Gibbs entropy $S = -k_{\rm B}\sum_i p_i \ln p_i$ does not change after a whole period so that $\Delta S_{\rm tot} = \Delta S_{\rm flux} = \int_0^{2\mathcal{T}_{\rm p}} dt\dot{S}_{\rm flux}$. Therefore, to get the fluctuation information of the total entropy, we can then apply the full counting statistics to count the flux entropy $s_{\rm flux} = \ln \frac{\Gamma_u^v(1-f_u^v)}{\Gamma_u^v f_u^v} = \varepsilon_0/T_u$ produced on each transition from the center level to both leads $v = {\rm L}, {\rm R}$ in each ensemble $u = {\rm A}, {\rm B}$.

In this way, the twisted transfer matrix with entropy counting becomes

$$\hat{H}_u = \begin{pmatrix} -K_u f_u & (\Gamma_u^{\rm L}+\Gamma_u^{\rm R})(1-f_u)e^{i\chi s_{\rm flux}} \\ (\Gamma_u^{\rm L}+\Gamma_u^{\rm R})f_u e^{-i\chi s_{\rm flux}} & -K_u(1-f_u) \end{pmatrix}.$$

Similar to approaches from Eq. (2) to Eq. (8) we obtain the total entropy change per period: $\Delta S_{\rm tot} = \Delta S_{\rm flux} = \langle s_{\rm flux}(2\mathcal{T}_{\rm p})\rangle - \langle s_{\rm flux}(0)\rangle$. Further, we have

$$\Delta S_{\rm tot} = \varepsilon_0 \frac{(f_{\rm A}-f_{\rm B})(T_{\rm A}-T_{\rm B})}{T_{\rm A}T_{\rm B}} \cdot \frac{(1-e^{-K_{\rm A}\mathcal{T}_{\rm p}})(1-e^{-K_{\rm B}\mathcal{T}_{\rm p}})}{(1-e^{-(K_{\rm A}+K_{\rm B})\mathcal{T}_{\rm p}})}. \quad (9)$$

This total entropy change shares the same behavior of transferred electron number Eq. (8), as depicted in Fig. 3, so we do not repeat the plotting here. Similarly, at slow switch limit $\mathcal{T}_{\rm p} \to \infty$, the entropy change per period is

$$\Delta S_{\rm tot} = \frac{\varepsilon_0(f_{\rm A}-f_{\rm B})(T_{\rm A}-T_{\rm B})}{T_{\rm A}T_{\rm B}}, \quad (10)$$

which is independent of period and has the same topological interpretation of Pancharatnam's geometric phase as that of the thermoelectric pumped electron. The nonequilibrium thermodynamic geometry is clearly illustrated in Fig. 4, where the entropy production is exactly the area enclosed by the thermodynamic cycle of GTEP. At fast switch limit $\mathcal{T}_{\rm p} \to 0$, the entropy change per period reads

$$\Delta S_{\rm tot} = \frac{\varepsilon_0 K_{\rm A}K_{\rm B}(f_{\rm A}-f_{\rm B})(T_{\rm A}-T_{\rm B})}{(K_{\rm A}+K_{\rm B})T_{\rm A}T_{\rm B}}\mathcal{T}_{\rm p}, \quad (11)$$

which is proportional to the period, so that the average entropy production rate $\Delta S_{\rm tot}/(2\mathcal{T}_{\rm p})$ is a period-independent constant. These similar behaviors and underlying physics between Eq. (8) and Eq. (9) [Eq. (6) and Eq. (10), Eq. (7) and Eq. (11)] indicate that the more the entropy dissipated into the environment (metallic leads), the farther the system will be pulled away from the equilibrium (more entropy changes), and thus the more the electron transfers can be generated.

We now briefly estimate the open-circuit voltage, $V_{\rm oc}$. Clearly, the maximum $V_{\rm oc}$ will be achieved in the largest asymmetric case $\Gamma_{\rm A}^{\rm L}/\Gamma_{\rm A}^{\rm R} \gg \Gamma_{\rm B}^{\rm L}/\Gamma_{\rm B}^{\rm R}$. Let us further assume that $+V_{\rm oc}/2$ is imposed on the left lead and $-V_{\rm oc}/2$ is imposed on the right one, and recall $T_{\rm A} > T_{\rm B}$. In the first half period, ensemble A, the electron transfers from the left lead to the central system ($\Gamma_{\rm A}^{\rm R} = 0$), carrying entropy $(\varepsilon_0 + eV_{\rm oc}/2)/T_{\rm A}$. In the second half period, ensemble B, the electron transfers from the central part to the right lead ($\Gamma_{\rm B}^{\rm L} = 0$), releasing entropy $(\varepsilon_0 - eV_{\rm oc}/2)/T_{\rm B}$. The reversibility of the charge transfer at the open-circuit condition requires zero entropy production, so that $(\varepsilon_0 + eV_{\rm oc}/2)/T_{\rm A} = (\varepsilon_0 - eV_{\rm oc}/2)/T_{\rm B}$. Therefore, we have the relation

$$V_{\rm oc} = 2\frac{\varepsilon_0}{e}\frac{T_{\rm A}-T_{\rm B}}{T_{\rm A}+T_{\rm B}}, \quad (12)$$

which is also confirmed numerically (not shown here). It indicates that increasing the temperature fluctuation and meanwhile decreasing the average temperature can increase the open-circuit voltage, which is upper bounded by $V_{\rm oc}^{\rm max} = 2\varepsilon_0/e$.

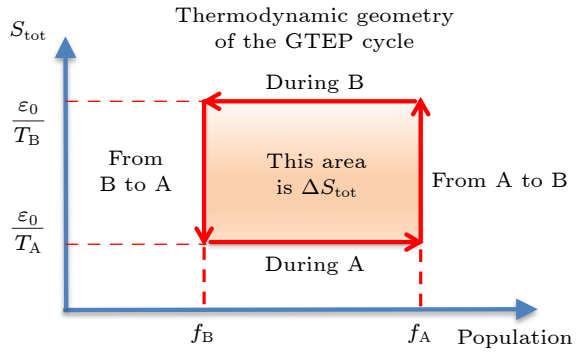

Fig. 4. Thermodynamic geometry of entropy production in the GTEP cycle in slow switch limit. The switch protocol forms a closed loop: when switching from ensemble B to A, the system's entropy switches from $\varepsilon_0/T_{\rm B}$ to $\varepsilon_0/T_{\rm A}$, while the population of the central level starts to relax from $f_{\rm B}$ to $f_{\rm A}$ during stage A in the large period limit. Then, when the system switches from A to B, the system's entropy changes from $\varepsilon_0/T_{\rm A}$ to $\varepsilon_0/T_{\rm B}$ and the population of the central level will relax from $f_{\rm A}$ to $f_{\rm B}$; so that the evolution of GTEP forms a closed thermodynamic cycle, whose area is $\Delta S_{\rm tot} = \varepsilon_0(\frac{1}{T_{\rm A}} - \frac{1}{T_{\rm B}})(f_{\rm A} - f_{\rm B})$, exactly as the same as the entropy production from the full counting statistics.

Finally, we provide realistic parameter estimates for the GTEP effect converted electricity. The real coupling rates are usually at the scale of GHz, indicating one electron hopping per nanosecond. We then can confer the unit GHz to the dimensionless couplings used for calculating Figs. 2 and 3. As such, the peak current $I_{\rm SC} = 0.04$ in Fig. 2 corresponds to $0.04 \times 1.6 \times 10^{-19}\,{\rm C}/10^{-9}\,{\rm s} = 6.4\,{\rm pA}$, and the average current per period at $Q/(2\mathcal{T}_{\rm p}) \approx 0.004$ in Fig. 3 corresponds to 0.64 pA. Considering the advantage of scalability in nanodevices, if we pack molecular quantum dots with spacing 50 nm between two metallic plate leads, we will have the packing density $4 \times 10^{10}/{\rm cm}^2$ that leads to the significant current density around the order of $0.1\,{\rm A/cm}^2$. Also, the output voltage can be further optimized in practice, e.g., in the molecular junction the energy gap between the LUMO and the lead's Fermi level is around $\varepsilon_0 = 2\,{\rm eV}$,[26,27] which compared to our used $\varepsilon_0 = 40\,{\rm meV}$ can further improve the output voltage

according to Eq. (12). Moreover, the temperature fluctuation in the industry or deep space, e.g., the satellite or the space station, can be as large as 100–500 K, which can generate even better electricity by the GTEP effect.

Although there is widespread demand in thermal energy science for both cost reductions and performance improvements, it is important in this stage to explore "out of the box" in principle. The GTEP effect reported here as the third way of thermal-electric conversion is such an attempt. In contrast to Seebeck and pyroelectric effects, GTEP effect is a consequence of the temperature-fluctuation-induced charge redistribution. This third way of thermal-electric conversion does not require neither polarized materials nor spatial temperature heterogeneity. It results from the fundamental nonequilibrium thermodynamic geometry[22,23] and has a deep connection to the topological geometric phase in non-Hermitian quantum mechanics.

Future extensions include the smooth and continuous temperature variation, macroscopic version of GTEP effect in bulk materials, thermo-spin conversion and pumping,[48–51] and complex-network-based thermal energy conversion,[52] where more detailed power and efficiency analysis should be desired. Also, exploring the geometric-phase-induced pumping effect in spatiotemporal metamaterials will be of great potential interest.[53–55] Moreover, multi-physics coupled transport will provide versatile opportunities for new types of thermo-electric conversion and vice versa. For example, Ref. [56] requires an electrochemical system combined with temperature fluctuations for heat energy harvesting. Based on the multi-caloric effect, such as elastocaloric effect,[57] electrocaloric effect,[58–64] many novel heat pumping devices based on periodic modulation have been proposed. The present work, however, depends neither on electrochemical systems nor on pyroelectric or other specific multi-caloric materials, but lays the foundation of understanding such temperature-fluctuation-induced electricity in nonequilibrium systems in a general way. We believe that, as human's ability to design and manipulate nano-systems is improving, the GTEP effect, as the third way of thermal-electric conversion, will provide the new means of energy harvesting to harness the ubiquitous temperature fluctuations in the world.

Acknowledgments. This work was supported by the National Natural Science Foundation of China (Grant No. 11935010), the Natural Science Foundation of Shanghai (Grant Nos. 23ZR1481200 and 23XD1423800), and the Opening Project of Shanghai Key Laboratory of Special Artificial Microstructure Materials and Technology.

References

[1] Chu S and Majumdar A 2012 *Nature* **488** 294
[2] Li N, Ren J, Wang L, Zhang G, Hänggi P, and Li B 2012 *Rev. Mod. Phys.* **84** 1045
[3] Lawrence Livermore National Laboratory, Estimated Energy Use in 2021 https://flowcharts.llnl.gov.
[4] DiSalvo F J 1999 *Science* **285** 703
[5] Spin Seebeck effect is also included here, which first converts the thermal difference into spin current and then into electric current, through the inverse spin Hall effect.
[6] Bell L E 2008 *Science* **321** 1457
[7] Tritt T M 2011 *Annu. Rev. Mater. Res.* **41** 433
[8] Shakouri A 2011 *Annu. Rev. Mater. Res.* **41** 399
[9] Lang S B 1974 *Sourcebook Pyroelectricity* (New York: CRC Press) vol 2
[10] Whatmore R 1986 *Rep. Prog. Phys.* **49** 1335
[11] Lang S B 2005 *Phys. Today* **58** 31
[12] Utilizing the ferro-paraelectric phase transition to generate electricity from temperature fluctuations also belongs to the pyroelectric effect.
[13] Sebald G, Guyomar D, and Agbossou A 2009 *Smart Mater. Struct.* **18** 125006
[14] Morozovska A, Eliseev E, Svechnikov G, and Kalinin S V 2010 *J. Appl. Phys.* **108** 042009
[15] Yang Y, Guo W, Pradel K C, Zhu G, Zhou Y, Zhang Y, Hu Y, Lin L, and Wang Z L 2012 *Nano Lett.* **12** 2833
[16] Yang Y, Wang S, Zhang Y, and Wang Z L 2012 *Nano Lett.* **12** 6408
[17] Yang Y, Jung J H, Yun B K, Zhang F, Pradel K C, Guo W, and Wang Z L 2012 *Adv. Mater.* **24** 5357
[18] Rogers J A and Paik U 2010 *Nat. Nanotechnology* **5** 385
[19] Seebeck T J 1822–1823 *Abhandlungen der Königlich Preussischen Akademie der Wissenschaften* (Berlin: Springer) p 265
[20] Brewster D 1824 *Edinburgh. J. Sci.* **1** 208
[21] Majumdar A 2013 *MRS Bull.* **38** 947
[22] Wang Z, Wang L, Chen J, Wang C, and Ren J 2022 *Front. Phys.* **17** 13021
[23] Wang Z, Chen J, and Ren J 2022 *Phys. Rev. E* **106** L032102
[24] Harman T, Taylor P, Walsh M, and LaForge B 2002 *Science* **297** 2229
[25] Dresselhaus M S, Chen G, Tang M Y, Yang R, Lee H, Wang D, Ren Z, Fleurial J P, and Gogna P 2007 *Adv. Mater.* **19** 1043
[26] Reddy P, Jang S Y, Segalman R A, and Majumdar A 2007 *Science* **315** 1568
[27] Lee W, Kim K, Jeong W, Zotti L A, Pauly F, Cuevas J C, and Reddy P 2013 *Nature* **498** 209
[28] Breuer H P, Petruccione F *et al.* 2002 *The Theory of Open Quantum Systems* (Oxford: Oxford University Press)
[29] Haug H, Jauho A P *et al.* 2008 *Quantum Kinetics in Transport and Optics of Semiconductors* (Berlin: Springer) vol 2
[30] Sze S M, Li Y, and Ng K K 2021 *Physics of Semiconductor Devices* (New York: John Wiley & Sons)
[31] Singh J 2005 *Smart Electronic Materials: Fundamentals and Applications* (Cambridge: Cambridge University Press)
[32] Pancharatnam S 1956 *Proc. Indian Acad. Sci. A* **44** 247
[33] Ben-Aryeh Y 2004 *J. Opt. B: Quantum Semiclass. Opt.* **6** R1
[34] Sinitsyn N and Nemenman I 2007 *Europhys. Lett.* **77** 58001
[35] Sinitsyn N 2009 *J. Phys. A* **42** 193001
[36] Ren J, Hänggi P, Li B *et al.* 2010 *Phys. Rev. Lett.* **104** 170601
[37] Ren J, Liu S, and Li B 2012 *Phys. Rev. Lett.* **108** 210603
[38] Chen T, Wang X B, and Ren J 2013 *Phys. Rev. B* **87** 144303
[39] Wang C, Ren J, and Cao J 2017 *Phys. Rev. A* **95** 023610
[40] Astumian R D and Hänggi P 2002 *Phys. Today* **55** 33
[41] Rahav S, Horowitz J, and Jarzynski C 2008 *Phys. Rev. Lett.* **101** 140602
[42] Sagawa T and Hayakawa H 2011 *Phys. Rev. E* **84** 051110
[43] Yuge T, Sagawa T, Sugita A, and Hayakawa H 2012 *Phys. Rev. B* **86** 235308
[44] Uchiyama C 2014 *Phys. Rev. E* **89** 052108
[45] Schnakenberg J 1976 *Rev. Mod. Physics* **48** 571
[46] Luo J L, Van den Broeck C, and Nicolis G 1984 *Z. Phys. B - Condens. Matter* **56** 165
[47] Seifert U 2005 *Phys. Rev. Lett.* **95** 040602

[48] Ren J 2013 *Phys. Rev. B* **88** 220406
[49] Ren J and Zhu J X 2013 *Phys. Rev. B* **88** 094427
[50] Ren J, Fransson J, and Zhu J X 2014 *Phys. Rev. B* **89** 214407
[51] Tang G, Chen X, Ren J, and Wang J 2018 *Phys. Rev. B* **97** 081407
[52] Wang L, Wang Z, Wang C, and Ren J 2022 *Phys. Rev. Lett.* **128** 067701
[53] Xu L, Xu G, Huang J, and Qiu C W 2022 *Phys. Rev. Lett.* **128** 145901
[54] Xu L, Xu G, Li J, Li Y, Huang J, and Qiu C W 2022 *Phys. Rev. Lett.* **129** 155901
[55] Lei M, Xu L, and Huang J 2023 *Mater. Today Phys.* **34** 101057
[56] Lee S W, Yang Y, Lee H W, Ghasemi H, Kraemer D, Chen G, and Cui Y 2014 *Nat. Commun.* **5** 3942
[57] Tusek J, Engelbrecht K, Eriksen D, Dall'Olio S, Tusek J, and Pryds N 2016 *Nat. Energy* **1** 16134
[58] Ma R, Zhang Z, Tong K, Huber D, Kornbluh R, Ju Y S, and Pei Q 2017 *Science* **357** 1130
[59] Wang Y, Zhang Z, Usui T, Benedict M, Hirose S, Lee J, Kalb J, and Schwartz D 2020 *Science* **370** 129
[60] Torell A, Lheritier P, Usui T, Nouchokgwe Y, Grard M, Bouton O, Hirose S, and Defay E 2020 *Science* **370** 125
[61] Meng Y, Zhang Z, Wu H, Wu R, Wu J, Wang H, and Pei Q 2020 *Nat. Energy* **5** 996
[62] Meng Y, Pu J, and Pei Q 2021 *Joule* **5** 780
[63] Cui H, Zhang Q, Bo Y, Bai P, Wang M, Zhang C, Qian X, and Ma R 2022 *Joule* **6** 258
[64] Qian X, Chen X, Zhu L, and Zhang Q M 2023 *Science* **380** eadg0902